

THE BRIGHTEST OF REIONIZING GALAXIES SURVEY: DESIGN AND PRELIMINARY RESULTS *

M. TRENTI

University of Colorado, Center for Astrophysics and Space Astronomy, 389-UCB, Boulder, CO 80309 USA

AND

L. D. BRADLEY

Space Telescope Science Institute, 3700 San Martin Drive Baltimore MD 21218 USA

AND

M. STIAVELLI

Space Telescope Science Institute, 3700 San Martin Drive Baltimore MD 21218 USA

AND

P. OESCH

Institute of Astronomy, ETH Zurich, CH-8093 Zurich, Switzerland

AND

T. TREU

Department of Physics, University of California, Santa Barbara, CA 93106-9530, USA

AND

R. J. BOUWENS

Astronomy Department, University of California, Santa Cruz, CA 95064, USA ; Leiden Observatory, University of Leiden, Postbus 9513, 2300 RA Leiden, Netherlands

AND

J. M. SHULL

CASA, Department of Astrophysics and Planetary Science, University of Colorado, 389-UCB, Boulder, CO 80309 USA

AND

J. W. MACKENTY

Space Telescope Science Institute, 3700 San Martin Drive Baltimore MD 21218 USA

AND

C. M. CAROLLO

Institute of Astronomy, ETH Zurich, CH-8093 Zurich, Switzerland

AND

G. D. ILLINGWORTH

Astronomy Department, University of California, Santa Cruz, CA 95064, USA

Draft version June 11, 2018

ABSTRACT

We present the first results on the search for very bright ($M_{AB} \approx -21$) galaxies at redshift $z \sim 8$ from the Brightest of Reionizing Galaxies (BoRG) survey. BoRG is a Hubble Space Telescope Wide Field Camera 3 pure-parallel survey that is obtaining images on random lines of sight at high Galactic latitudes in four filters (F606W, F098M, F125W, F160W), with integration times optimized to identify galaxies at $z \gtrsim 7.5$ as F098M-dropouts. We discuss here results from a search area of approximately 130 arcmin² over 23 BoRG fields, complemented by six other pure-parallel WFC3 fields with similar filters. This new search area is more than two times wider than previous WFC3 observations at $z \sim 8$. We identify four F098M-dropout candidates with high statistical confidence (detected at greater than 8σ confidence in F125W). These sources are among the brightest candidates currently known at $z \sim 8$ and approximately ten times brighter than the $z = 8.56$ galaxy UDFy-38135539. They thus represent ideal targets for spectroscopic followup observations and could potentially lead to a redshift record, as our color selection includes objects up to $z \sim 9$. However, the expected contamination rate of our sample is about 30% higher than typical searches for dropout galaxies in legacy fields, such as the GOODS and HUDF, where deeper data and additional optical filters are available to reject contaminants.

Subject headings: galaxies: high-redshift — galaxies: evolution

1. INTRODUCTION

*BASED ON OBSERVATIONS MADE WITH THE NASA/ESA HUBBLE SPACE TELESCOPE, WHICH IS OPERATED BY THE ASSOCIATION OF UNIVERSITIES FOR RESEARCH IN ASTRONOMY, INC., UNDER NASA CONTRACT NAS 5-26555. THESE OBSERVATIONS ARE ASSOCIATED WITH

PROGRAMS 11700, 11702
Electronic address: trenti@colorado.edu

The installation of Wide Field Camera 3 (WFC3) on the *Hubble Space Telescope* opened new possibilities for discovery of $z > 7$ galaxies. Observations on the GOODS and HUDF fields have increased the sample of $z \gtrsim 7$ candidates to $N > 100$ (Oesch et al. 2010b; Bouwens et al. 2010a; McLure et al. 2010; Finkelstein et al. 2010; Wilkins et al. 2010). Legacy multi-wavelength coverage on these fields and the improved spatial resolution of WFC3 enabled preliminary characterization of the properties of these sources in terms of stellar mass, stellar populations and size (Oesch et al. 2010a; Bouwens et al. 2010c; Labbé et al. 2010).

However, the current search area, while containing deep and ultradeep data, is modest (approximately 60 arcmin²) and located within or around a single GOODS field. This provides significant uncertainty in the number density of $z \gtrsim 7$ galaxies owing to small-number statistics and cosmic variance (Bouwens et al. 2010a). This is especially severe at the bright end of the luminosity function (LF), where sources are most clustered and least abundant (e.g., see Trenti & Stiavelli 2008). These WFC3 observations suggest that the galaxy LF evolves sharply from $z \sim 6$ to $z \sim 8$, particularly at the bright end (Bouwens et al. 2010a). Such trend is consistent with the underlying evolution of the dark matter halo mass function, which predicts well the LF evolution (Trenti et al. 2010), but stronger observational constraints on M_* are needed.

Reducing uncertainty on the number density of bright $z \sim 8$ sources also benefits the determination of the LF faint-end slope α . Fits to a Schechter (1976) LF, $\phi(L) = \phi_*(L/L_*)^\alpha \exp(-L/L_*)$, have a strong degeneracy between characteristic luminosity $M_* = -2.5 \log_{10}(L_*)$ and α (Bouwens et al. 2007; Trenti & Stiavelli 2008). Measuring α is fundamental to assess whether galaxies emit enough photons to reionize the Universe (Bunker et al. 2004; Chary 2008; Henry et al. 2009; Trenti et al. 2010; Robertson et al. 2010). Ground-based programs (Ouchi et al. 2009; Castellano et al. 2010) place useful constraints on M_* at slightly lower redshift ($z \lesssim 7$), but the impact of large-scale structure remains a concern, because all these searches are within legacy fields.

To complement the existing campaigns aimed at searching for $z \gtrsim 7.5$ galaxies, we introduce here the HST BoRG (Brightest of Reionizing Galaxies) survey. BoRG is based on pure-parallel observations with HST-WFC3 while the telescope is pointing to a primary spectroscopic target (typically a foreground high- z QSO). Because lines of sight are independent and well separated on the sky, cosmic variance is negligible. In contrast, cosmic variance introduces approximately 25% uncertainty, in addition to Poisson noise, in the number counts of $z \gtrsim 6$ galaxies for both the GOODS and the HUDF surveys. A survey with independent lines of sight provides an unbiased characterization of the LF bright-end with errors equivalent to those of a continuous survey of about twice its area (Trenti & Stiavelli 2008).

The preliminary BoRG dataset discussed here contains 29 lines of sight for a total of approximately 130 arcmin², more than twice the area of the HUDF and GOODS-ERS observations in Bouwens et al. (2010a). This wide area allows us to identify galaxies that are good candidates for follow-up spectroscopic observations; all $z \sim 8$ galaxies

in BoRG are significantly brighter than UDFy-38135539 for which Lehnert et al. (2010) reported detection of Ly α emission at $z = 8.56$.

Section 2 of this paper introduces the BoRG survey. Data reduction is discussed in Section 3. Section 4 presents our selection strategy along with estimates of contamination. Preliminary results are presented in Section 5 and compared with an independent analysis by Yan et al. (2010). Section 6 summarizes and concludes. We adopt a standard WMAP7 cosmology (Komatsu et al. 2010) and the AB magnitude scale (Oke 1974).

2. SURVEY DESIGN

The BoRG survey is designed to identify bright ($m_{F125W} \lesssim 27$) high-redshift galaxies from their broad-band colors using the Lyman-Break technique (Steidel et al. 1996). The primary aim of the survey is to select $z \gtrsim 7.5$ galaxies as F098M dropouts. Two near-IR filters (F125W and F160W) are used for source detection. One optical filter (F606W) is used to control the primary source of contamination from lower redshift $z \sim 1.5$ interlopers (see Section 4). As we detail below, the survey was designed to minimize the probability that artifacts and low-redshift interlopers may pass our selection criteria.

Parallel opportunities of program GO/PAR 11700 are at least three orbits in length (mostly 3-5 orbits). Each individual visit has a particular duration determined by the details of its primary program (see Table 1). The exposure time between filters has been allocated by keeping the relative depths approximately constant, within the constraints imposed by the primary program. In calculating the relative exposure times, we also took into account the effect of Galactic reddening. We used the primary line of sight as a proxy for the extinction expected in WFC3 images. From the reddening map of Schlegel et al. (1998) and extinction law of Cardelli et al. (1989), we derived the extinction in each band.

Dithering in pure-parallel observations is determined by the primary program, so it is usually absent because primary observations are spectroscopic. This introduces some challenges in the data analysis, especially with respect to systematic errors introduced by the detector, namely hot pixels and detector persistence in the IR channel, which arises following observations of targets that saturate the detector (Dressel et al. 2010). The latter is of particular concern because of the possibility of introducing an artificial coherent signal into the detection band(s) for F098M-dropouts, thereby leading to false candidates. To minimize the impact of persistence, we ensured that every observation of Program 11700 in either F125W or F160W is preceded in the same orbit by a comparably long F098M exposure. When possible, F160W observations follow F125W. As detector persistence decays over time (with approximate power-law behavior), any saturated target observed in a previous visit affects most the initial part of the pure-parallel orbit, which is the exposure in the dropout filter. With this strategy, persistence features are guaranteed not to contaminate the dropout selection. To ensure good sampling of the IR exposures, we opted for reading every 100 s (SPARS100). While the majority of cosmic rays are rejected by the calibration pipeline, owing to the multi-

ple non-destructive readouts of WFC3, a small fraction may survive in the calibrated image. We thus split the total integration in each IR filter into at least two individual exposures. F606W exposures are split in $N_s \geq 3$ sequences (each 500 – 900 s) for cosmic-ray rejection, except for shallower fields, where $N_s = 2$ if the total F606W integration is less than 1000 s. Our design choices are aimed at maximizing the data quality, although a small price is paid in the term of signal-to-noise ratio. For example, our strategy to “shield” F125W and F160W observations from persistence by means of a F098M exposure carries some overhead because filter rotation happens during the observation window.

We also consider a small number of fields from another pure-parallel program with the same IR filters but with F600LP instead of F606W (GO/PAR 11702, PI Yan). Images in program GO/PAR 11702 are not characterized by the optimization described above; for a given pointing, F098M exposures tend to be in different orbits than the redder IR filters. In addition, some IR filters only have a single exposure and both SPARS100 and SPARS200 sampling is used. Overall, this makes the additional dataset potentially more vulnerable to spurious sources.

3. DATA REDUCTION AND CATALOG CONSTRUCTION

The images were reduced using standard techniques. For the WFC3/IR data, we recalibrated the raw data using `calwfc3` using the most up-to-date reference files and our own custom flat fields generated by median stacking of publicly available WFC3/IR data in F098M, F125W, and F160W. We used SExtractor (Bertin & Arnouts 1996) to background subtract the FLT files prior to running `multidrizzle` (Koekemoer et al. 2002). The background levels were stored in the headers of each FLT file and are subsequently used by `multidrizzle` for cosmic-ray rejection. The individual exposures were aligned and drizzled on a common 0.08 arcsec/pixel scale using `multidrizzle`.

To identify F098M-dropout sources we first constructed a preliminary catalog with SExtractor, then we checked the source S/N reported by SExtractor and normalized the input rms maps if needed. Finally we reran SExtractor to obtain the final source catalog. Below we describe these steps.

In each field, we identified sources from the F125W image using SExtractor in dual image mode. We required at least 9 contiguous pixels with $S/N \geq 0.7$ for the preliminary catalog.

Multidrizzle introduces correlated noise in the images (Casertano et al. 2000). To derive realistic errors, one needs to rescale the rms map by measuring the noise in areas of size comparable to observed galaxies. Therefore, we selected 400 random pointings at distance $d > 0.4''$ from detected sources. There we performed circular aperture photometry (radius $r = 0.32''$) with SExtractor in dual image mode. We used a synthetic detection image with artificial sources at the location of the random pointings and the actual images as photometry frames. We normalized the rms map of each filter requiring that, for these sky apertures, the median of the nominal error reported by SExtractor (FLUXERR_APER) is equal to the rms of the measured flux (FLUX_APER). This re-

sults in an average multiplication of the rms maps by 1.5 for F606W, by 1.15 for F098M and by 1.1 for F125W and F160W.

After rescaling the rms maps, we reran SExtractor to create a final version of the catalogs. To include a source, we required detection with $S/N > 8$ in F125W and $S/N > 3$ in F160W for ISOMAG fluxes. Colors were computed from ISOMAG measurements. Total magnitudes were defined as AUTOMAG.

We derived median 5σ sensitivities in a circular aperture with radius $r = 0.32''$ (median exposures times also listed) of $m_{F606W} = 26.9$ ($t_{exp} = 2647$ s), $m_{F600LP} = 26.4$ ($t_{exp} = 2334$ s), $m_{F098M} = 26.8$ ($t_{exp} = 4515$ s), $m_{F125W} = 26.7$ ($t_{exp} = 2205$ s), $m_{F160W} = 26.3$ ($t_{exp} = 1405$ s). Table 1 reports the individual field sensitivities. We used photometric zero points 26.08, 25.85, 25.68, 26.25, 25.96 respectively for F606W, F600LP, F098M, F125W, F160W (Dressel et al. 2010).

4. SELECTION OF $Z \sim 8$ GALAXY CANDIDATES

Candidate galaxies at $z \gtrsim 7.5$ are selected using broadband colors analogous to other $z \gtrsim 6$ galaxy surveys (Oesch et al. 2010b; Bouwens et al. 2010b). In short, we search for objects that have a strong break in the filter corresponding to the redshifted Ly α absorption at $z \gtrsim 7.5$. We use F098M as the dropout filter, requiring:

$$m_{F098M} - m_{F125W} \geq 1.75. \quad (1)$$

If $S/N < 1$ in F098M, we replace the measured flux with its 1σ limit. Furthermore, to remove lower redshift red and/or obscured contaminants, we require that $m_{F125W} - m_{F160W}$ is moderately red at most:

$$m_{F125W} - m_{F160W} < 0.02 + 0.15 \times (m_{F098M} - m_{F125W} - 1.75). \quad (2)$$

The third condition we impose is a conservative non-detection at 1.5σ in the optical band available (F606W or F600LP).

These conditions have been chosen by optimizing the selection efficiency of genuine $z \gtrsim 7$ galaxies while minimizing contamination from low-redshift galaxies and cool stars. Our IR color-color selection window is shown in Fig. 1, along with typical colors for possible galaxy contaminant sources. The figure is based on a library of 10 million galaxy spectral energy distributions constructed using different star-formation histories, metallicities, and dust content (see Oesch et al. 2007). Fig. 1 also shows the expected redshift distribution of Lyman Break galaxies entering our selection window.

The availability of high-quality deep optical data appears to be the limiting factor in the rejection of low-redshift galaxy contaminants. In fact, passively evolving galaxies at $z \sim 1.5$ can contaminate the F098M-dropout selection when their 4000 Å/Balmer break is misidentified as Ly α break if the data are not sufficiently deep to detect these sources in the optical bands (see also Henry et al. 2009; Capak et al. 2009). We estimate approximately 30% contamination using the GOODS-ERS data (Program 11359) which include F098M imaging. We estimate this number as follows: from the Bouwens et al. (2010a) data reduction we first identify F098M-dropouts with $m_{F125W} \leq 27$ using the selection discussed above, but considering a version of the GOODS F606W image degraded to a 5σ limit $m_{F606W} = 27.2$

to match the relative F125W vs. F606W BoRG depth. We then check for contaminants by rejecting F098M-dropouts with $S/N > 2$ in either B , V , or i (at their full depth). Approximately 30% contamination is in good agreement with the estimate based on the application of the color selection to our library of SED models (Figure 1).

Cool stars are another possible source of contamination. Our survey area is large and probes lines of sight at different Galactic latitudes. Thus, we cannot argue that they are unlikely to be present based on their rarity as in the HUDF (Bouwens et al. 2010b). However, based on the brown dwarf spectra of Reid et al. (2001) and on the colors for L and T dwarfs measured by Knapp et al. (2004), the use of F098M as a dropout filter is efficient at rejecting brown dwarf stars; the expected colors of these contaminants are well separated from our selection window (see Figure 1). In addition, owing to the high-resolution of WFC3, it is expected that all the brightest galaxies at $z \gtrsim 7$ will be extended sources (Oesch et al. 2010a), providing a further diagnostic to identify Galactic stellar contaminants. Our bright dropouts ($m_{F125W} \leq 26$) have low values of the SExtractor Stairity parameter (see Table 2), hence they are consistent with being resolved. Overall, we do not expect this source of contamination to be significant.

5. SAMPLE OF $Z \sim 8$ CANDIDATES

Four objects satisfy our dropout selection, all from BoRG fields. Their photometry is reported in Table 2. Figures 2-3 show the candidates' images. Here we discuss each candidate, critically assessing its likelihood to be at $z \gtrsim 7.5$, starting with the least robust. Three of these four objects have been identified as F098M-dropouts by an independent analysis of our data (Yan et al. 2010). All fields with candidates contain at least two exposure frames per filter (taken in different orbits). We verified that candidates are detected in each individual F125W and F160W frame at S/N ratio consistent with scaling from the total to the individual exposure time.

5.1. *BoRG66_1741-1157*

This object is detected in $F125W$ with $S/N = 8.7$, but only marginally in $F160W$ ($S/N = 3.3$). Hence, it has the bluest $J - H$ color of the sample. With $Y - J = 1.9 \pm 0.6$, it lies at the edge of our dropout selection window, and its membership in the sample of $z \gtrsim 7.5$ candidates could be the result of photometric scatter. Its blue color could be due to contribution from strong Ly α emission in F125W. This object is not in the Yan et al. (2010) sample.

5.2. *BoRG1k_0847-0733*

This candidate also lies at the edge of the selection window, and its inclusion in the sample could be due to photometric scatter in either $Y - H$ or $J - H$ color (with $\sim 60\%$ probability if errors are symmetric). There are hints of flux at optical wavelength: $(S/N)_{F606W} = 1.3$ ($S/N \geq 1.3$ has probability $p \leq 6.6\%$ for Gaussian noise). The F606W exposure is shallow (Table 1): $t = 1260$ s (5σ mag limit 26.3). The dropout filter has a marginal detection ($S/N_{F098M} = 2.4$). Because of these multiple bits of circumstantial evidence, we consider the object a

low-probability $z \gtrsim 7.5$ candidate, more likely to be a passive $z \sim 1.5$ galaxy.

5.3. *BoRG0t_0958-0641*

BoRG0t_0958-0641 is the faintest candidate in the sample, but has $(S/N)_{F125W} > 8$ and $(S/N)_{F160} = 6.8$ because of the significant exposure time in this field (Table 1). Data from programs 11700 and 11702 cover the region at slightly different orientations, providing some dithering. The candidate is well within the color-color selection window for $z \gtrsim 7.5$ galaxies (Figure 1). Yan et al. (2010) do not consider this object a strong $z > 7.5$ candidate because they claim variability on the three-day timescale of the observations (see their Figure 4). We performed aperture photometry ($r = 0.32''$) at the source location for the three epochs, and find no evidence of variability in F125W (measuring $m = 26.7, 26.8, 26.8$ with typical 1σ sky uncertainty of approximately 0.35 mag in each frame). We see evidence of variability in F160W at about 2σ confidence: $m = 26.2, 26.9, 27.2$ with 1σ error of approximately 0.35 mag. Closer examination highlights potential data quality issues. In the first epoch, the readouts of the F160W ramp for pixels within the source jump between readout 8 and 9, indicating a cosmic ray hit. In the second epoch, there is a hot pixel located within this source. Because of the stable photometry in F125W, we consider intrinsic variability unlikely, although further observations would be useful to clarify the nature of this source.

5.4. *BoRG58_1787-1420*

This is the most robust candidate of the sample, with all its properties fully consistent with being a $z \gtrsim 7.5$ galaxy. The measured colors are well within the selection window, even after taking into account 1σ errors. The object lies on the $z \gtrsim 7.5$ galaxy tracks. There is no flux at optical wavelength ($(S/N)_{F606W} < 0$).

6. DISCUSSION AND CONCLUSIONS

In this paper we discuss the preliminary results from the BoRG survey on the search of bright $z \gtrsim 7.5$ galaxies identified as F098M-dropouts using HST WFC3 data. By analyzing 29 independent lines of sight, we identify four dropouts with $(S/N)_{F125W} > 8\sigma$. Two objects lie near the selection window border, and they are possibly low-redshift interlopers scattered into the selection (but it is similarly likely that photometric scatter removes objects from the sample). The remaining candidates satisfy all the expected properties for $z \gtrsim 7.5$ objects with high confidence.

Detailed discussion on the implications for the evolution of the galaxy LF are deferred to a future paper (L. D. Bradley et al., in preparation). There, we will also attempt to extend the detection of dropouts to fainter limits and carry out artificial source recovery simulations to estimate the effective volume of the BoRG survey as a function of magnitude. Here we consider a magnitude limit $m_{F125W} \leq 26.2$ (equivalent to $M \leq -20.9$), where completeness is close to unity in all regions of the BoRG data not occupied by a foreground object. To estimate our effective area, we masked all pixels at distance $d \leq 0.4''$ from a pixel belonging to the SExtractor segmentation map and counted the remaining pixels, deriving an effective search area of approximately

97 arcmin². Further assuming a pencil-beam geometry with $7.5 \leq z \leq 8.5$, we derive a comoving volume of $2.3 \times 10^5 \text{ Mpc}^3$. From the best fit $z = 8$ LF derived by Bouwens et al. (2010a) based on ERS and HUDF data, we expect $N \sim 2.5$ galaxies with $M \leq -20.9$ in our search area. Three candidates at $m_{F125W} \leq 26.2$ are fully consistent with this expectation, even after taking into account a contamination rate of approximately 30% from low- z galaxies (Section 4), but alternative models cannot be strongly ruled out. For constant $\alpha = -2.0$ and $\phi_* = 0.38 \times 10^{-3} \text{ Mpc}^{-3}$ (Bouwens et al. 2010a), we derive $M_* = -20.2 \pm 0.3$ (68% confidence). Quadrupling the BoRG area would allow us to set $\Delta M_* < 0.3$ at 99% confidence. Similar future pure-parallel observations (e.g. GO/PAR 12286 PI Yan) will contribute toward this goal by approximately doubling the current search area.

Finally, BoRG58_1787-1420 represents an ideal can-

didate for follow-up spectroscopic investigations. This galaxy is about ten times brighter than UDFy-38135539 for which Lehnert et al. (2010) claimed detection of Ly α emission at $z = 8.56$. BoRG58_1787-1420 could potentially yield a more secure line identification if the equivalent width is similar to the $\sim 1900 \text{ \AA}$ of UDFy-38135539, or alternatively a comparable line flux (approximately $6 \times 10^{-18} \text{ erg s}^{-1} \text{ cm}^{-2}$) for a 200 \AA equivalent width. In addition, from Trenti et al. (2010), we derive $M_h \sim 7 \times 10^{11} M_\odot$ as the host-halo mass for BoRG58_1787-1420. This galaxy likely lives in an overdense region of the universe, where the IGM is ionized at early times, facilitating escape (and detection) of the Ly α radiation.

We thank the referee for useful suggestions. We acknowledge grants HST-GO-11563 and HST-GO-11700.

REFERENCES

- Bertin, E. & Arnouts, S. 1996, *A&AS*, 117, 393
- Bouwens, R. J., Illingworth, G. D., Franx, M. & Ford, H. 2007, *ApJ*, 670, 928
- Bouwens, R. J., Illingworth, G. D., Oesch, P. A., Labbe, I., Trenti, M., van Dokkum, P., Franx, M., Stiavelli, M., Carollo, C. M., Magee, D., & Gonzalez, V. 2010a, arXiv:1006.4360
- Bouwens, R. J., Illingworth, G. D., Oesch, P. A., Stiavelli, M., van Dokkum, P., Trenti, M., Magee, D., Labbé, I., Franx, M., Carollo, C. M., & Gonzalez, V. 2010b, *ApJ*, 709, L133
- Bouwens, R. J., Illingworth, G. D., Oesch, P. A., Trenti, M., Stiavelli, M., Carollo, C. M., Franx, M., van Dokkum, P. G., Labbé, I., & Magee, D. 2010c, *ApJ*, 708, L69
- Bunker, A. J., Stanway, E. R., Ellis, R. S., McMahon, R. G. 2004, *MNRAS*, 355, 374
- Capak, P., Mobasher, B., Scoville, N. Z., McCracken, H., Ilbert, O., Salvato, M., Menendez-Delmestre, K., Aussel, H., Carilli, C., Civano, F., Elvis, M., Giavalisco, M., Jullo, E., Kartaltepe, J., Leauthaud, A., Koekemoer, A. M., Kneib, J., LeFloche, E., Sanders, D. B., Schinnerer, E., Shioya, Y., Shopbell, P., Taniguchi, Y., Thompson, D., & Willott, C. J. 2009, arXiv:0910.0444
- Cardelli, J. A., Clayton, G. C., & Mathis, J. S. 1989, *ApJ*, 345, 245
- Casertano, S., de Mello, D., Dickinson, M., Ferguson, H. C., Fruchter, A. S., Gonzalez-Lopezlira, R. A., Heyer, I., Hook, R. N., Levay, Z., Lucas, R. A., Mack, J., Makidon, R. B., Mutchler, M., Smith, T. E., Stiavelli, M., Wiggs, M. S. & Williams, R. E. 2000, *AJ*, 120, 2747
- Castellano, M., Fontana, A., Boutsia, K., Grazian, A., Pentericci, L., Bouwens, R., Dickinson, M., Giavalisco, M., Santini, P., Cristiani, S., Fiore, F., Gallozzi, S., Giallongo, E., Maiolino, R., Mannucci, F., Menci, N., Moorwood, A., Nonino, M., Paris, D., Renzini, A., Rosati, P., Salimbeni, S., Testa, V., & Vanzella, E. 2010, *A&A*, 511, A20+
- Chary R.-R. 2008, *ApJ*, 680, 32
- Dressel, L., Wong, M.H., Pavlovsky, C., and Long, K. et al. 2010. Wide Field Camera 3 Instrument Handbook, Version 2.1 (Baltimore: STScI)
- Finkelstein, S. L., Papovich, C., Giavalisco, M., Reddy, N. A., Ferguson, H. C., Koekemoer, A. M., & Dickinson, M. 2010, *ApJ*, 719, 1250
- Henry, A. L., Siana, B., Malkan, M. A., Ashby, M. L. N., Bridge, C. R., Chary, R.-R., Colbert, J. W., Giavalisco, M., Teplitz, H. I., McCarthy, P. J. 2009, *ApJ*, 697, 1128
- Koekemoer, A. M., Fruchter, A. S., Hook, R. N., & Hack, W. 2002, in *The 2002 HST Calibration Workshop: Hubble after the Installation of the ACS and the NICMOS Cooling System*, ed. S. Arribas, A. Koekemoer, & B. Whitmore, 337–+
- Komatsu, E., Smith, K. M., Dunkley, J., Bennett, C. L., Gold, B., Hinshaw, G., Jarosik, N., Larson, D., Nolte, M. R., Page, L., Spergel, D. N., Halpern, M., Hill, R. S., Kogut, A., Limon, M., Meyer, S. S., Odegard, N., Tucker, G. S., Weiland, J. L., Wollack, E., & Wright, E. L. 2010, arXiv:1001.4538
- Knapp, G. R. et al. 2004, *AJ*, 127, 3553
- Labbé, I., Gonzalez, V., Bouwens, R. J., Illingworth, G. D., Oesch, P. A., van Dokkum, P. G., Carollo, C. M., Franx, M., Stiavelli, M., Trenti, M., Magee, D., & Kriek, M. 2010, *ApJL*, 708, 26
- Lehnert, M. D., Nesvadba, N. P. H., Cuby, J., Swinbank, A. M., Morris, S., Clément, B., Evans, C. J., Bremer, M. N., & Basa, S. 2010, *Nature*, 467, 940
- Malhotra, S., Rhoads, J. E., Pirzkal, N., Haiman, Z., Xu, C., Daddi, E., Yan, H., Bergeron, L. E., Wang, J., Ferguson, H. C., Gronwall, C., Koekemoer, A., Kummel, M., Moustakas, L. A., Panagia, N., Pasquali, A., Stiavelli, M., Walsh, J., Windhorst, R. A., & di Serego Alighieri, S. 2005, *ApJ*, 626, 666
- McLure, R. J., Dunlop, J. S., Cirasuolo, M., Koekemoer, A. M., Sabbie, E., Stark, D. P., Targett, T. A., & Ellis, R. S. 2010, *MNRAS*, 403, 960
- Oesch, P. A., Bouwens, R. J., Carollo, C. M., Illingworth, G. D., Trenti, M., Stiavelli, M., Magee, D., Labbé, I., & Franx, M. 2010a, *ApJ*, 709, L21
- Oesch, P. A., Bouwens, R. J., Illingworth, G. D., Carollo, C. M., Franx, M., Labbé, I., Magee, D., Stiavelli, M., Trenti, M., & van Dokkum, P. G. 2010b, *ApJ*, 709, L16
- Oesch, P. A., Stiavelli, M., Carollo, C. M., Bergeron, L. E., Koekemoer, A. M., Lucas, R. A., Pavlovsky, C. M., Trenti, M., Lilly, S. J., Beckwith, S. V. W., Dahlen, T., Ferguson, H. C., Gardner, J. P., Lacey, C., Mobasher, B., Panagia, N., & Rix, H. 2007, *ApJ*, 671, 1212
- Oke, J. B. 1974, *ApJS*, 27, 21
- Ouchi, M., Mobasher, B., Shimasaku, K., Ferguson, H. C., Fall, S. M., Ono, Y., Kashikawa, N., Morokuma, T., Nakajima, K., Okamura, S., Dickinson, M., Giavalisco, M., & Ohta, K. 2009, *ApJ*, 706, 1136
- Reid, I. N., Burgasser, A. J., Cruz, K. L., Kirkpatrick, J. D., & Gizis, J. E. 2001, *AJ*, 121, 1710
- Robertson, B. E., Ellis, R. S., Dunlop, J. S., McLure, R. J. & Stark, D. P., 2010, *Nature*, 468, 49
- Schlegel, D. J., Finkbeiner, D. P., & Davis, M. 1998, *ApJ*, 500, 525
- Steidel, C. C., Giavalisco, M., Pettini, M., Dickinson, M., & Adelberger, K. L. 1996, *ApJ*, 462, L17+
- Trenti, M. & Stiavelli, M. 2008, *ApJ*, 676, 767
- Trenti, M., Stiavelli, M., Bouwens, R. J., Oesch, P., Shull, J. M., Illingworth, G. D., Bradley, L. D., & Carollo, C. M. 2010, *ApJ*, 714, L202
- Wilkins, S. M., Bunker, A. J., Ellis, R. S., Stark, D., Stanway, E. R.; Chiu, K., Lorenzoni, S. & Jarvis, M. J. 2010, *MNRAS*, 403, 938
- Yan, H., Yan, L., Zamojski, M. A., Windhorst, R. A., McCarthy, P. J., Fan, X., Röttgering, H. J. A., Koekemoer, A. M., Robertson, B. E., Davé, R., & Cai, Z. 2010, ArXiv:1010.2261

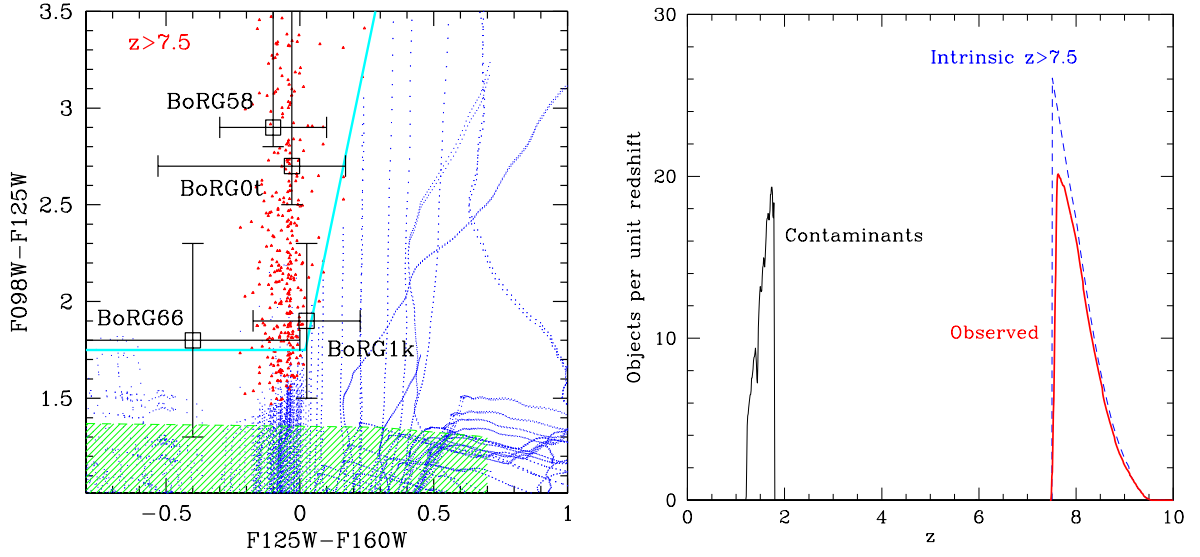


FIG. 1.— Left: F098M-dropouts color-color selection. Black squares indicate our four $z > 7.5$ candidates (with 1σ error bars). Cyan lines denote selection window. Blue dots are simulated low-redshift interlopers. Red triangles $z > 7.5$ galaxies. L, T dwarf stars from Knapp et al. (2004) occupy green shaded area (see Bouwens et al. 2010a). Right: Expected redshift distribution for candidates within the selection window (red: $z > 7.5$ galaxies; black: low- z interlopers). Blue-dotted line shows redshift distribution for luminosity-limited selection of $z > 7.5$ galaxies (the color-color selection rejects some sources).

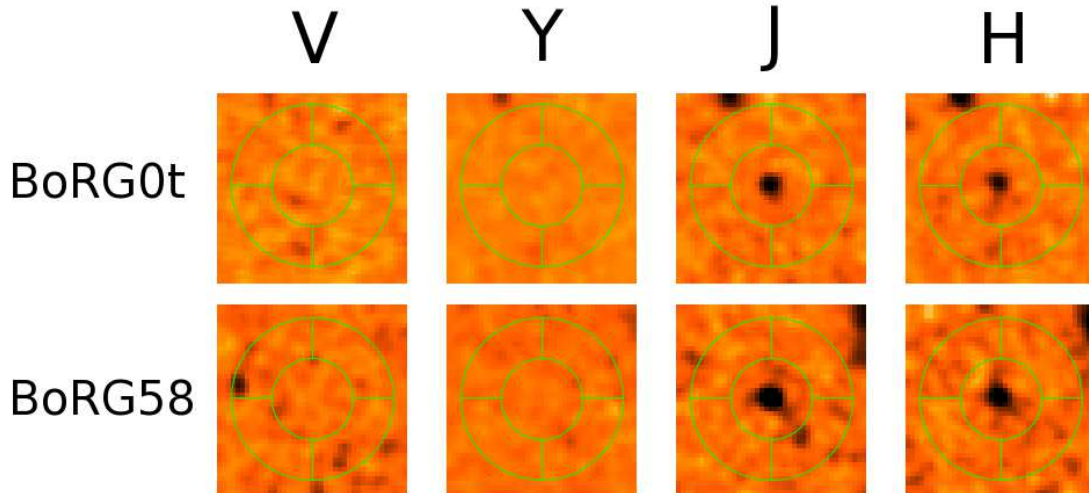


FIG. 2.— Region ($3.2'' \times 3.2''$) surrounding the most robust BoRG F098M-dropout candidates (left to right: F606W, F098M, F125W, F160W).

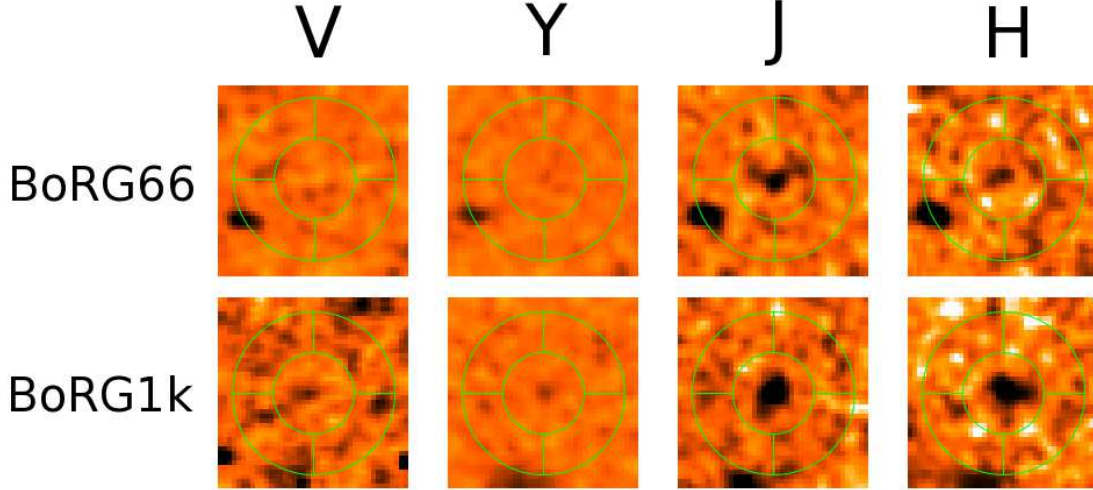


FIG. 3.— As in Fig. 2, but showing the least robust BoRG dropouts.

TABLE 1
BoRG FIELDS LOCATION, EXPOSURE TIMES AND 5σ MAGNITUDE LIMITS ($r = 0.32''$)

Field	RA	DEC	F125W		F160W		F098M		F606W		F600LP	
	[deg]	[deg]	t [s]	m_{lim}	t [s]	m_{lim}	t [s]	m_{lim}	t [s]	m_{lim}	t [s]	m_{lim}
BoRG93	99.286	-75.307	2412	26.6	1612	26.0	6218	26.8	4290	26.9		
BoRG81	88.277	-64.091	2612	26.9	2012	26.3	6418	27.0	3624	27.1		
BoRG73	136.403	2.925	2709	27.1	1906	26.6	5518	27.0	3106	27.0		
BoRG70	157.712	38.059	1506	26.3	1306	26.1	3109	26.4	1815	26.4		
BoRG66	137.284	-0.030	1806	26.8	1006	26.1	3909	26.9	2650	26.9		
BoRG58	219.230	50.719	2509	27.0	1806	26.6	4912	27.1	2754	26.8		
BoRG49	191.184	33.937	1506	26.6	1106	26.2	3409	26.8	1789	26.8		
BoRG45	141.390	40.005	1106	26.1	903	25.9	2806	26.2	1276	26.1		
BoRG39	138.567	28.363	2206	26.9	1706	26.5	4615	26.9	2571	26.9		
BoRG30 ¹	125.011	23.536	703	26.1	703	25.8	3109	26.5	2556	26.8		
BoRG2t ¹	95.903	-64.528	1206	26.4	503	25.6	1806	26.4	2133	26.7		
BoRG2n	84.879	-64.153	2309	26.6	1406	26.3	4112	26.6	3171	27.1		
BoRG2k	95.952	-64.665	1206	26.6	906	26.0	2909	26.7	2135	26.9		
BoRG1v	187.473	7.825	1806	25.9	1406	25.6	4112	26.0	2436	26.6		
BoRG1r	140.403	45.087	2106	26.6	1706	26.3	4812	26.7	2708	26.6		
BoRG1n	122.086	39.759	2206	26.5	1406	26.0	4612	26.5	2600	26.7		
BoRG1k	247.889	37.610	1206	26.6	906	26.1	2909	26.8	1260	26.3		
BoRG0y	177.963	54.684	2809	27.1	1906	26.7	6021	27.1	2898	27.1		
BoRG0j	178.180	0.933	2209	26.7	1606	26.5	4515	26.8	2647	26.8		
BoRG0c	118.986	30.718	1906	26.6	1406	26.3	4712	26.8	2600	26.9		
BoRG0g	124.834	49.183	1206	26.5	806	25.8	3009	26.6	1908	26.5		
BoRG0p	182.358	45.723	3709	27.3	2909	27.0	13729	27.6	2707	27.0	2234	26.4
BoRG0t	117.707	29.282	5115	27.2	3912	26.9	18641	27.5	2826	26.9	3752	26.7
yan11	190.553	57.268	2509	26.9	2309	26.6	5215	27.0			2800	26.5
yan19	204.200	-0.462	1203	26.7	1203	26.3	6818	27.1			2270	26.2
yan24	33.408	12.914	1403	26.0	1403	25.8	2806	26.0			2294	26.0
yan28	141.379	44.427	1603	26.8	1403	26.5	6012	27.0			2374	26.4
yan32	205.128	41.386	3206	27.2	2806	27.0	17435	27.6			3810	26.8
yan51	231.038	9.905	1603	26.6	1303	26.2	8718	27.0			2078	26.3

NOTE. — Survey area: approximately 130 arcmin². Effective area for F098M-dropout detection: approximately 97 arcmin².¹ Data missing due to scheduling constraint/conflict.

TABLE 2
BoRGs F098M-DROPOUTS

	RA	DEC	m_J	IR-Colors Y-J	J-H	S/N ^a			Stellarity	
						V	Y	J	H	
BoRG66_1741-1157	137.2732	-0.0297	26.2 ± 0.2	1.9 ± 0.6	-0.4 ± 0.4	-0.8	2.1	8.7	3.3	0.01
BoRG1k_0847-0733 ⁺	247.8968	+37.6039	25.5 ± 0.1	1.9 ± 0.4	0.0 ± 0.2	1.3	2.4	11.4	7.4	0.03
BoRG0t_0958-0641 ^{+b}	117.7142	+29.2715	26.7 ± 0.2	≥ 2.6	$0.0^{+0.2}_{-0.5}$	-0.9	0.1	8.6	6.8	0.79
BoRG58_1787-1420 ⁺	219.2107	+50.7260	25.8 ± 0.1	≥ 2.8	-0.1 ± 0.2	-1.4	-0.7	13.2	8.0	0.36

NOTE. — Photometric properties of candidates and their coordinates (Deg, J2000 system). Magnitude m_J is AUTOMAG from SExtractor. Colors are derived from ISOMAG (fluxes below 1σ have been replaced with 1σ limit). SExtractor Stellarity parameter also reported.

⁺ In Yan et al. (2010) catalog.

^a Negative S/N is due to negative sky-subtracted flux within the photometric aperture used.

^b Also available: F600LP filter with $S/N = -0.2$.